NANO LETTERS

Letter

pubs.acs.org/NanoLett

Wiring-up Carbon Single Wall Nanotubes to Polycrystalline Inorganic Semiconductor Thin Films: Low-Barrier, Copper-Free Back Contact to CdTe Solar Cells

Adam B. Phillips,[†] Rajendra R. Khanal,[†] Zhaoning Song,[†] Rosa M. Zartman,[†] Jonathan L. DeWitt,[†] Jon M. Stone,[†] Paul J. Roland,[†] Victor V. Plotnikov,[‡] Chad W. Carter,[‡] John M. Stayancho,[‡] Randall J. Ellingson,[†] Alvin D. Compaan,[†,‡] and Michael J. Heben*,[†]

[†]Wright Center for Photovoltaics Innovation and Commercialization, Department of Physics and Astronomy, School of Solar and Advanced Renewable Energy, University of Toledo, Toledo, Ohio 43606, United States

[‡]Lucintech Incorporated, Toledo, Ohio 43606, United States

Supporting Information

ABSTRACT: We have discovered that films of carbon single wall nanotubes (SWNTs) make excellent back contacts to CdTe devices without any modification to the CdTe surface. Efficiencies of SWNT-contacted devices are slightly higher than otherwise identical devices formed with standard Au/Cu back contacts. The SWNT layer is thermally stable and easily applied with a spray process, and SWNT-contacted devices show no signs of degradation during accelerated life testing.

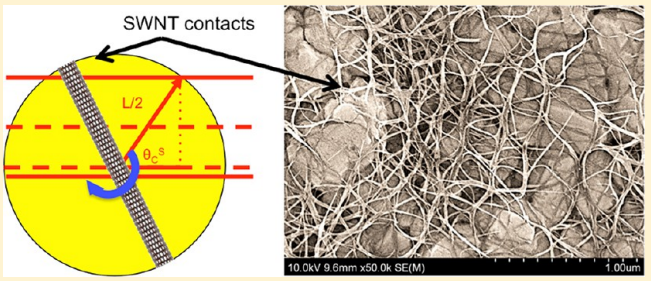

KEYWORDS: *CdTe, photovoltaic, nanotube, thin film, back contact*

With a 1.45 eV band gap, a high absorption coefficient, and proven low-cost, high-volume manufacturing, CdTe-based photovoltaic (PV) technology accounted for more than 7% of the 100 GW of solar power generating capacity that was installed worldwide by the end of 2012.[1,2] New efficiency records for CdTe PV of 19.6%[3] and 16.1%[4] have been established recently at the cell and module levels, respectively, and current manufacturing costs for CdTe ($0.64/$W_P$)[5] are lower than all other PV technologies. However, due to a high electron affinity, a valence band edge that is 5.75 eV[6,7] below the vacuum level (E_{Vac}), and a low p-type carrier density[8,9] on the order of 10^{14} cm^{-3}, it is difficult to make low resistance electrical back contacts to CdTe solar cells.

Copper doping of CdTe assists in forming back contacts to CdTe devices in both laboratory studies and commercial applications, but Cu is known to diffuse through the p-type CdTe absorber to the n-type CdS window layer and produce junction-shunting pathways.[10−12] As a result, the efficiency of commercial CdTe modules degrades by 0.7% per year.[13] Even this slow degradation leads to panels that produce only 85% of the rated output at the end of a 25 year lifetime. In addition to slow degradation, Cu-related instabilities necessitate a 4−7% derating of the module's rated capacity at the factory due to rapid degradation that occurs in the first 1−3 years.[13] If both types of degradation could be eliminated, the levelized cost of electricity (LCOE)[14] could be reduced by 12% without any other changes in the device architecture or manufacturing flow.[15] CdTe PV technology already competes favorably with silicon photovoltaics and coal-fired power plants in hot climates and locations with high electricity prices, respectively, due to a low LCOE. A lower LCOE would further accelerate the adoption of PV technology and help the world address the urgent need for CO_2 free power.

Because of the detrimental effects of Cu, several material systems have been investigated for use as the back contact for Cu-free CdTe devices. Most of this work has been focused on modifying the barrier between the CdTe and the metal electrode through reduction of the space charge region thickness by including a p-doped semiconductor layer such as Sb_2Te_3,[16,17] ZnTe,[18,19] or MoO_X[20,21] on the CdTe back surface. Alternatively, indium tin oxide[22] has also been used. While some success has been achieved, in general these back contact methods result in lower device efficiency[17,22] and poor thermal stability;[17,21,23] however, high efficiency and thermal stability has been achieved using Mo/Sb_2Te_3 .[17,23]

Here, we demonstrate that carbon single-wall nanotube (SWNTs) films can make a high-performance electrical back contact to CdTe solar cells without the use of Cu. Back contacts formed with SWNT films showed improved open-circuit voltage (V_{OC}) in comparison to cells fabricated with standard Au/Cu back contacts and, once overcoated with a thin metal layer, the solar-to-electric conversion efficiency was

Received: July 18, 2013
Revised: October 7, 2013

   dx.doi.org/10.1021/nl402659c | *Nano Lett.* XXXX, XXX, XXX−XXX

higher as well. The results are understood by considering that individual SWNTs within the film extend through the film's thickness and make barrier-less contacts to individual CdTe grains in the active layer of the device. Perhaps most significantly, in contrast to contacts that employ Cu, the SWNT contacts show no sign of band alignment degradation after high-temperature thermal stress testing, suggesting that long-term performance degradation can be eliminated. Importantly, SWNT contacts can be applied with an atmospheric pressure ultrasonic spray process that is amenable to large areas and can be integrated with existing manufacturing lines at low cost.

CdTe/CdS photovoltaic devices were grown by magnetron sputtering on soda-lime glass coated with a thin fluorine-doped tin oxide (FTO) transparent conducting layer. Magnetron sputtering was chosen as the deposition technique to produce films with compact grains and a relatively smooth surface.[24,25] Vapor phase $CdCl_2$ activation was employed to promote grain growth, release interfacial strain, and facilitate sulfur and tellurium mixing at the CdTe/CdS interface. After $CdCl_2$ activation, CdTe samples were used without any further processing. The deposited n-type CdS and p-type CdTe layers were typically 80 nm and 1.5 μm thick, respectively. Because our focus is on the performance of the SWNT back contact, no efforts were made to optimize the efficiency of the CdTe/CdS devices by, for example, increasing the CdTe thickness, thinning the CdS layer, adding optimized buffer layers, adjusting the $CdCl_2$ treatment, or using low-iron glass and high-performance transparent conductors to increase light transmission into the cells. Consequently, the typical efficiency for these devices with a standard Au/Cu back contact under AM1.5G simulated solar radiation was 10%. For comparison, optimized CdTe devices fabricated by the UT/Lucintech group on low-iron, soda-lime glass have reached 14.5% efficiency.[26]

SWNTs were produced by a modified laser vaporization technique[27] and purified by a version of the process developed by Nishide et al.[28] SWNT films (100 nm thick) were prepared on the back surface of the CdTe devices by both membrane transfer[29] and ultrasonic spraying.[30] Both techniques yielded similar results. Sprayed films were prepared from SWNTs suspended in aqueous sodium dodecylbenzene sulfonate (SDBS) dispersions, and the SDBS was removed by successive washes in deionized water. Since no acids were employed, the as-prepared thin films were not significantly doped. More details regarding preparation of the films can be found in the Supporting Information. This report focuses on sprayed films due to the inherent scalability of the ultrasonic spray deposition process.

Results and Discussion. Representative current density versus voltage (J/V) curves for CdTe devices prepared with different back contacts are shown in Figure 1a, and key device parameters are presented in Table 1. An evaporated, 30 nm thick Au contact produced a J/V response under simulated AM1.5 radiation with a short circuit current density (J_{SC}) of 19.5 mA/cm^2. This value is good for the device construction, but the V_{OC} and efficiency (η) are poor. The V_{OC} is low because, even with a relatively high work function (φ = 5.1 eV), Au creates an undesired Schottky barrier at the back contact that impedes majority carrier transport out the back of the device.[11,31] When a 3 nm layer of Cu is evaporated before the Au, and the device is subsequently heated for 30 min at 150 °C in air to promote diffusion of Cu into the CdTe, the V_{OC} improves from 665 to 757 mV and the efficiency improves from

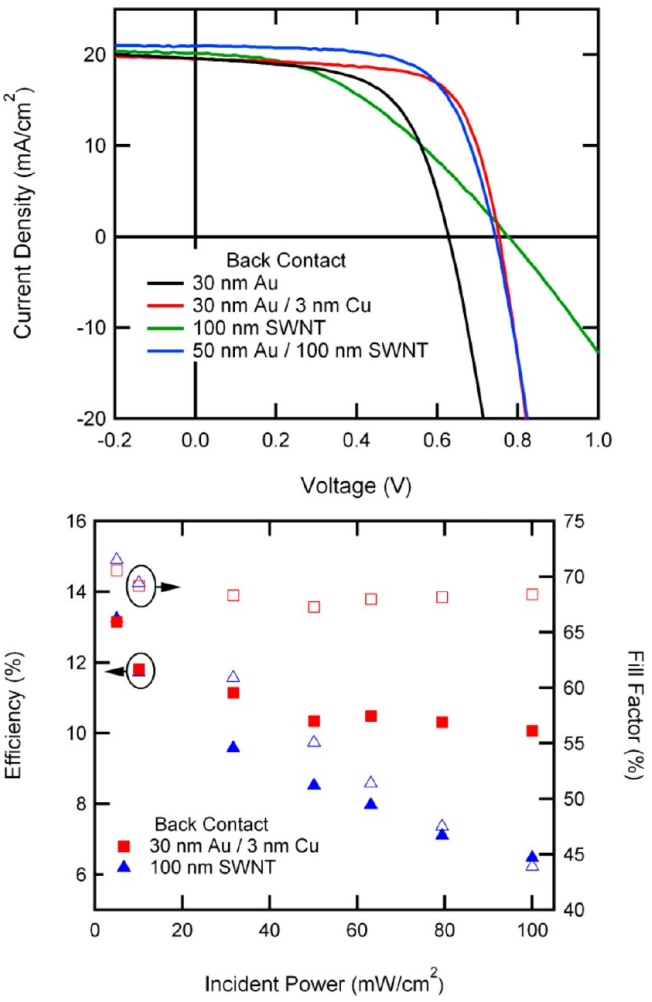

Figure 1. (a) Current density versus bias voltage (J/V) measurements of CdTe devices with Au, Au/Cu, SWNT, and Au/SWNT back contacts obtained under simulated AM1.5G solar spectrum. (b) Light intensity dependence of efficiency (left) and fill factor (right) for CdTe devices with Au/Cu and SWNT back contacts.

7.8 to 10.2%. The dramatic improvement in performance with the addition of Cu highlights the importance of eliminating the ~300 mV back barrier typical of gold and other contacts.[11] As indicated previously, it is difficult to make a low-resistance electrical contact to p-type CdTe due to a low carrier concentration and an energetically deep valence band. This difficulty is typically overcome by (i) introduction of extrinsic doping at the CdTe back surface to reduce the space charge region thickness and allow defect-assisted carrier tunneling, or (ii) introducing another p-type semiconductor that can be more readily doped and mediate the contact between the high resistivity CdTe and a metal electrode.[9,32] The inclusion of Cu at the CdTe back surface is thought to perform both functions. With the postdeposition heat treatment, Cu diffuses and reacts with the CdTe surface to produce a higher doping level as well as an intermediary Cu_2Te phase. The Au/Cu contact is often used in laboratory environments while commercial contacts employ a thin layer of Cu overcoated with a less expensive oxidation resistant metal such as Cr.[33]

Figure 1a also shows J/V curves for a device finished with a pure 100 nm SWNT film and a second device having a 100 nm SWNT film overcoated with 50 nm of Au. Surprisingly, the device with the neat SWNT film shows the highest V_{OC} (778

dx.doi.org/10.1021/nl402659c | Nano Lett. XXXX, XXX, XXX−XXX

Table 1. Average J/V Parameters for 18 CdTe Devices before and after Heating

back contact	V_{OC} (volts)	J_{Sc} (mA/cm^2)	fill factor (%)	efficiency (%)	series resistance (Ω-cm^2)
		As Prepared			
Au	0.665 ± 0.75%	19.58 ± 2.3%	62.04 ± 1.7%	7.80 ± 3.1%	5.18 ± 5.2%
Au/Cu	0.757 ± 0.40%	19.52 ± 1.5%	69.00 ± 2.5%	10.20 ± 3.4%	4.12 ± 10%
SWNT	0.778 ± 0.77%	20.07 ± 3.1%	39.15 ± 12%	6.15 ± 15%	18.86 ± 9.1%
Au/SWNT	0.746 ± 0.53%	21.12 ± 1.5%	66.05 ± 2.1%	10.40 ± 1.1%	4.74 ± 13%
		After Heat Treatment (300 °C in Argon for 10 min)			
Au	0.499 ± 1.6%	19.73 ± 2.2%	60.34 ± 1.6%	5.94 ± 2.5%	3.93 ± 5.6%
Au/Cu	0.696 ± 1.7%	17.64 ± 1.3%	63.83 ± 1.4%	7.83 ± 2.3%	6.58 ± 7.0%
SWNT	0.783 ± 1.3%	14.00 ± 7.5%	28.45 ± 1.9%	3.12 ± 8.7%	46.50 ± 23%
Au/SWNT[a]	0.773 ± 0.51%	21.15 ± 1.3%	67.21 ± 2.1%	10.99 ± 2.8%	6.29 ± 16%

[a]Au films were applied to heated SWNT films. Heat treatment of Au/SWNT electrodes resulted in data similar to that found for heated Au contacts.

mV). The Au/SWNT contact was not heated after Au deposition, and the SWNT films were only heated as required during the SWNT spraying (140 °C), surfactant removal (50 °C), and film drying steps (80 °C). Although the spraying temperature is comparable to the temperature required to produce diffusion with a Au/Cu contact, the SWNT contact is expected to be thermally stable since no metals are present and the temperature is too low to initiate oxidation. The stability of the back contact is further demonstrated in experiments in which samples were heated to 300 °C (vide infra). The high V_{OC} indicates that the band alignment energetics at the SWNT/CdTe interface produce a low barrier to majority carrier flow without the need for introduction of Cu species. The fill factor (FF) for the neat SWNT film is, however, quite low (39%), so the photovoltaic conversion efficiency is also low (6.15%). Because a single 1.0 mm diameter spring-loaded pin collects current from the entire device area, the low FF is presumably due to the significant sheet resistance of the SWNT film (250 Ω/sq, measured on glass). Overcoating the SWNT film with 50 nm of Au reduces the effective sheet resistance to ~1 Ω/sq and the FF improves dramatically. In fact, the efficiency is found to be higher than in the Au/Cu reference device (10.4 vs 10.2%, respectively).

The curves in Figure 1a are representative of hundreds of individual devices that were examined for each type of back contact. The devices compared in a given data set were prepared from 1″ x 1″ samples that were cut from larger 3″ x 5.5″ plates. Each 1″ x 1″ sample yielded 24 individual 3 mm × 3 mm devices after laser scribing. With this approach, variation in device performance due to factors other than the back contact formulation could be determined. Table 1 shows PV performance parameters for a data set obtained with samples from a single CdTe plate. In this case, the 3 worst and 3 best devices from a 1″ x 1″ sample were eliminated and average data for 18 devices is presented. The average results are consistent with the representative curves displayed in Figure 1a, and the very tight spread in the obtained parameters indicates the reproducibility of these experiments.

To verify that the sheet resistance of the SWNT films limits the performance of the devices before application of the Au layer, we examined the J/V behavior for Au/Cu and SWNT contacted devices as a function of light intensity. For a Au/Cu device, the FF and η remain nearly constant as the intensity is reduced from 100 to 50 mW/cm^2 (Figure 1b). Equation 1 shows the relationship between J and V for a solar cell when series (R_S) and shunt (R_{Sh}) resistances are explicitly considered

$$J = J_{ph} - J_0\left(\exp\left[\frac{V + JR_s}{nkT}\right] - 1\right) - \frac{V + JR_s}{R_{Sh}} \quad (1)$$

Here, J_{Ph} is the light generated photocurrent, J_0 is the reverse saturation current, k is Boltzmann's constant, T is the temperature, and n is the diode quality factor. The lack of change in the FF and η while J_{Ph} is reduced by a factor of 2 suggests that the voltage drop across the series resistance (JR_S) at these light intensities is small in comparison to the bias voltage. This view is consistent with the relatively low series resistances for these samples, which is associated primarily with the resistance in the TCO layer (Table 1). Both the FF and η improve significantly as the light intensity is reduced below 50 mW/cm^2, perhaps due to an increased shunt resistance associated with a reduced photoconductivity in the CdS material.[34] Turning to the data for the SWNT back contact, the FF and η are observed to be a strong function of light intensity over the entire experimental range (Figure 1b). Once again, the photogenerated current is reduced as the light intensity is reduced, but in this case the voltage drop across a larger R_S (Table 1) is more significant. At 10 mW/cm^2, the voltage drop across R_S at the maximum power point becomes less than 10% of V_{OC} and the characteristics of the two devices become quite similar. At the lowest intensities (<10 mW/cm^2) the FF and η of the SWNT-contacted device actually exceeds that of the Au/Cu device. Thus, we can conclude that devices with neat SWNT contacts are limited in performance by the series resistance associated with lateral charge collection in the SWNT film. Evidently, there is little or no barrier to majority carrier flow at the SWNT/CdTe interface, and the application of a thin metal film on top of the SWNT layer only provides needed lateral conductivity to compensate for the film's high sheet resistance.

The wavelength dependence of the carrier collection efficiency was examined by comparing external quantum efficiency (EQE) measurements of devices with Au/Cu, SWNT, and Au/SWNT back contacts (Figure 2a). The EQE responses were, overall, quite similar demonstrating that the carrier collection efficiencies are essentially the same in all three types of devices. The current densities were low for these measurements so sheet resistance limitations were not encountered for the SWNT contact without Au. The substantial loss in QE between 400 to 550 nm is due to absorption in the relatively thick CdS layer and differences in the curves can be attributed to small CdS thickness variations. Reduction in the collection efficiency at longer wavelengths (550−800 nm) is associated with reflection from and absorption in the FTO/glass stack (see Supporting Informa-

dx.doi.org/10.1021/nl402659c | Nano Lett. XXXX, XXX, XXX−XXX

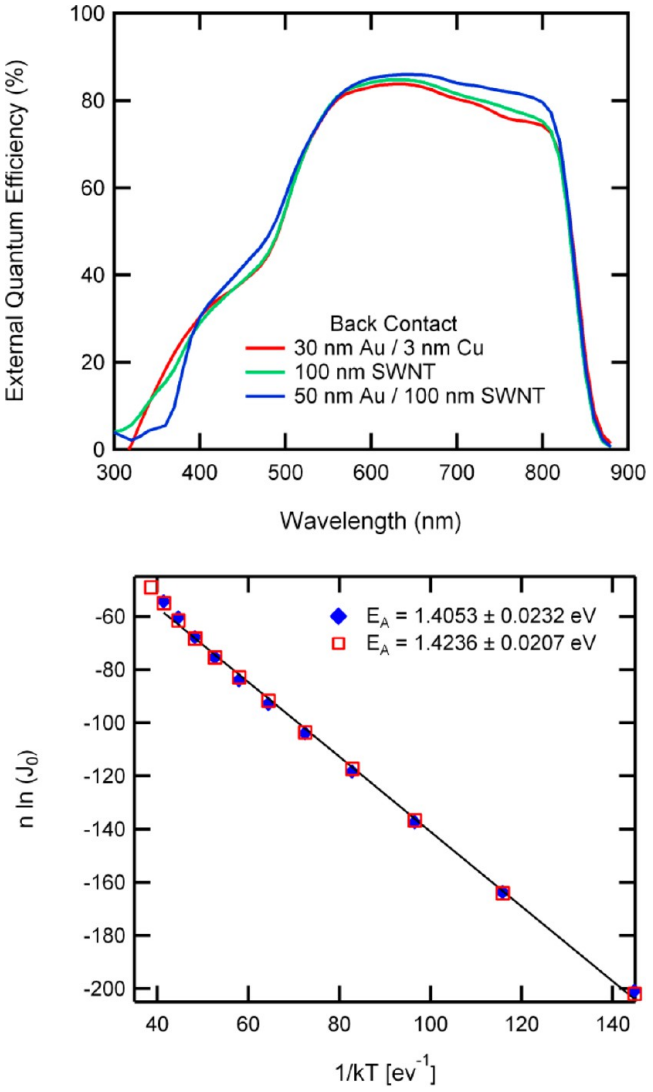

Figure 2. (a) External quantum efficiency for CdTe devices with Au/Cu, SWNT, and Au/SWNT back contacts. (b) Plot of $n \ln J_0$ vs $1/kT$ for CdTe devices with Au/Cu and Au/SWNT back contacts from 80 to 280 K . E_A was determined by a linear regression fit to the data, as explained in the text.

tion). Interestingly, the collection of carriers generated at the longest wavelengths (700−800 nm) is more efficient when SWNT are included in the device, suggesting a slower recombination velocity for minority carriers that are generated near the back contact. The long wavelength response is further improved when Au is applied to the SWNT layer. In contrast to the variation in EQE that may be seen at the short wavelengths, the performance improvement at long wavelengths with a Au overcoat is consistently observed and mirrored in the J_{SC} gains seen for Au/SWNT contacts (Table 1). However, the 5−10% improvement in the EQE in the 700−800 nm range cannot be directly ascribed to light reflected back from the Au or SWNT films since less than 1% of the incident light in this wavelength range makes it to the back contact (Supporting Information Figure S2). Clearly, more study is required to understand the origin of this improvement.

To gain more insight, J/V curves were measured for illuminated Au/Cu and Au/SWNT devices over a temperature range spanning from 80 to 300 K. The J/V curves at each temperature were fit to eq 1 to extract the temperature-dependent values of J_0 and n. The temperature dependence of J_0 may be used to evaluate the activation energy (E_a) for carrier recombination according to eq 2 where J_{00} is a prefactor that may be assumed to be temperature independent for our purposes[35]

$$J_0 = J_{00} \exp\left[\frac{-E_a}{nkT}\right] \quad (2)$$

Figure 2b shows a plot of $n \ln J_0$ versus $1/kT$ for devices with Au/Cu and Au/SWNT back contacts from which the apparent activation energy for carrier recombination can be evaluated. In both cases, E_a is near the band gap of the CdTe, establishing that the dominant recombination mechanism is the same in both devices and not a function of the back contact.

To investigate the structural characteristics of the SWNT/CdTe contact, scanning electron microscopy (SEM) was performed. At a relatively low acceleration potential (2 kV, Figure 3a) SEM shows a 100 nm SWNT film deposited on CdTe to be comprised of a fairly dense and tangled web of individual SWNTs and SWNT bundles. Interestingly, when the accelerating potential was increased to 10 kV and the wavelength of the incident electrons was reduced, the SWNT film became partially transparent and the underlying CdTe grains could be imaged (Figure 3b). For comparison, a bare CdTe surface is shown in Figure 3c. Evidently, the SWNT film acts as a blanket that covers and conforms to the topography of the polycrystalline CdTe thin film. Figure 3d shows an SEM image of a SWNT film after deposition of 30 nm of Au. In this case, we see 50−100 nm Au particles, suggesting that all of the deposited Au remains on the surface of the SWNT film. There is evidence that the Au decorates the SWNT bundles but the deposited Au does not wet or penetrate the SWNT film, consistent with previous studies.[36] Surprisingly, this relatively small amount of superficial metal is able to dramatically improve the device efficiency by reducing R_S (Table 1).

While considering how SWNTs form a low barrier contact to p-CdTe, it is instructive to review related experimental work with graphite and graphene. Graphite pastes have been used to contact CdTe PV devices but, as with Au contacts, diffusion of dopant metals such as Cu, Hg, and Sb was required to create a low back barrier.[37] Similarly, graphene has also been employed but, once again, Cu is always required.[38−40] Neither graphite nor graphene by themselves has been successfully employed as a low barrier back contact to CdTe solar cells, as expected due to their relatively low work function (φ = 5.0 eV).[41] The curvature and chirality possibilities for sp^2-bonded carbon atoms in SWNTs gives rise to both metallic (m-SWNTs) and semiconducting (s-SWNTs) species. In similarity to graphite and graphene, the work function for m-SWNTs is 5 eV below E_{Vac}.[42] However, the s-SWNTs in our samples have band gaps that range from 0.7−0.9 eV. With heavy p-type doping, E_F for SWNTs can be near the valence band edges of the tubes, which sit 5.35−5.45 eV below E_{Vac}. Thus, the electrochemical potential of the electrons that are presented by the SWNT layer to the CdTe contact could be considerably more negative than what is possible with either pure graphite or graphene.

To develop a better understanding of the electrical properties of the contact, the structural characteristics of the film need to be more thoroughly considered. Clearly, the properties of the SWNT layer are significantly different from those in a conventional, dense metal or semiconductor PV device layer.

dx.doi.org/10.1021/nl402659c | Nano Lett. XXXX, XXX, XXX−XXX

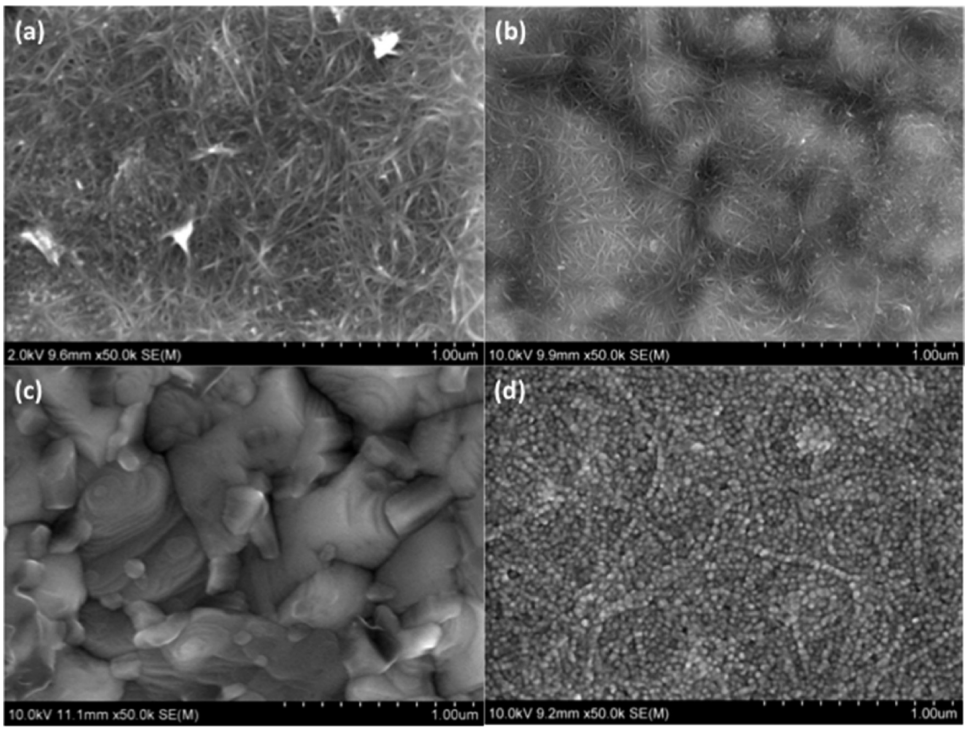

Figure 3. (a) SEM image of the SWNT/CdTe device at an accelerating voltage of 2 kV. (b) SEM image of the SWNT/CdTe device at 10 kV. (c) SEM image of the bare CdTe surface at 10 kV. (d) SEM image of the SWNT surface after Au deposition at 10 kV.

Charge transport is ballistic within individual SWNTs while long-range conduction is impeded by the multitude of tube−tube junctions that are present in a film.[43] Further complexity arises because the film is porous and comprised of s-SWNTs and m-SWNTs in a ratio of approximately 2 to 1.[44] The SEM images of Figure 3 make it clear that the SWNT film cannot be treated as a homogeneous layer with isotropic properties. Some ordering of the SWNTs within the film might be expected if low energy configurations could be sampled during a slow deposition process,[45] but deposition via spray or membrane transfer in our laboratories is done at a relatively high rate. In the absence of any suggestion of ordering we instead assume that the SWNTs are randomly oriented within the film. With random orientation, we expect that some tubes, whether individualized or in bundles, will extend across the thickness of the film and "span" internally from one surface of the film to the other.

To estimate the number of nanotubes that span a film of thickness T, we consider a rigid nanotube of length L and the surface area of a sphere swept-out by rotating it through all angles about its midpoint. For a SWNT with a midpoint that is located on the midplane of the film, the probability (P_S) that both ends of a tube will be outside the film is given by the fraction of the surface area of the rotational sphere that is outside one surface of the film. A more complete treatment of the problem (see Supporting Information) allows for the tube midpoints to be located anywhere throughout the film's thickness. In this case, P_S is given by eq 3

$$P_S = \frac{\frac{\pi}{8}L - \frac{T}{2}}{\frac{\pi}{8}L + \frac{T}{2}} \tag{3}$$

Using previous results for SWNTs prepared similarly,[30] we take L to be 500 nm. Thickness T was determined to be 100 nm from optical profilometry and absorption spectroscopy measurements. With these values, we determine that ∼60% of the SWNTs extend through the thickness of the film. The total number of SWNTs that span the film per unit area can be estimated using eq 4

$$n = V_f \frac{4T}{\pi D^2 L} \tag{4}$$

Here, V_f is the volume fraction occupied by the SWNTs and D is the SWNT diameter. Taking D to be 1.6 nm to account for 1/2 of a van der Waals spacing around each tube, and V_f to be 56%[30] we estimate that the number density of SWNTs spanning a 100 nm film, that is, the product of n times P_S, is 3.51×10^4 μm^{-2}. Note that this analysis is consistent with 2D conductivity because $L \gg T$ and all SWNTs are actually confined to the film.[30] In a 2D limit that might be achieved with layer-by-layer build-up of SWNT rafts, no SWNTs would extend across the film. Though clearly inconsistent with the SEM images in Figure 3, such a configuration would result in poor transport perpendicular to the film and much higher values of R_S even after deposition of gold. However, R_S of SWNT-contacted devices is low after a thin Au layer is applied and comparable to R_S for the Au/Cu contact (Table 1). Consistently, the temperature dependence of R_S for a device with a Au/SWNT contact varied by only ±5% from 80 to 300 K, while tube−tube transport would exhibit a variation of at least a factor of 2 over a similar temperature range.[43,46]

SWNTs are quite flexible and with $L \approx 5T$ could span between the surfaces of a film several times. Alternatively, if a tube traverses the film thickness only once, there would be multiple points at which it could be contacted at the surfaces of the film. The value of L used here is a mean value from the log-normal distribution of lengths produced by sonication,[30] so significantly more than half of the tubes are longer than L. This

dx.doi.org/10.1021/nl402659c | Nano Lett. XXXX, XXX, XXX−XXX

consideration leads to a higher density of spanning tubes. On the other hand, the SEM images of Figure 3 show that the SWNT layers are not entirely conformal to the nooks and crannies between CdTe grains. This consideration reduces the fraction of spanning tubes that could produce contacts to the CdTe. In any case, the highly idealized rigid-rod approximation indicates that a large number of nanotubes span the SWNT film. If even 1% of the tubes that span the film contact the underlying CdTe, several hundred contacts could be made to each 1 μm-sized CdTe grain.

Regardless of the exact contact density there is clearly intimate physical contact and strong adhesion of the SWNT to the CdTe. Efforts to remove the SWNT layer from the smooth CdTe surface with adhesive tapes in a pull test were completely unsuccessful when the SWNT layers were devoid of graphite impurities. The microscopic aspects of the film adhesion are not well understood at this time but may be associated with charge transfer interactions between SWNTs and semiconductor surfaces.[47]

At the specific sites where SWNTs contact the individual CdTe grains there will be nanoscale junctions with differing electronic properties depending on whether the contacting SWNTs possess metallic or semiconducting character. In fact, due to the evidently large contact density each individual grain will likely be simultaneously "wired-up" by both s- and m-SWNTS. The characteristics of each type of contact can be considered separately.

The work function of m-SWNTs is similar to that of graphite (5 eV), so the m-SWNTs are expected to form junctions with the CdTe that are rectifying without dopants such as Cu or Hg. The work function for m-SWNTs is less than Au's work function, so the loss in V_{OC} in the J/V curves should be more pronounced in comparison to the Au contact (see data in Figure 1). Device modeling with SCAPS[48] software indicated that, in similarity to Au, there was a significant barrier to hole transport at the back contact in both forward and reverse biases. Consequently, one can tentatively conclude that m-SWNTs do not assist in creating the excellent SWNT back contact. This conclusion is further supported by density functional theory (DFT) calculations that were performed for SWNTs interacting with InAs surfaces (vide infra).[49]

Turning to consideration of the s-SWNTs, for the diameters used here the valence band edges are located 5.35 to 5.45 eV below E_{Vac}. With a propensity for p-type doping,[50] one may expect that the low-lying valence bands of s-SWNTs afford a good opportunity to make a low barrier contact to p-CdTe. SCAPS modeling was once again performed to investigate the band diagram for devices with s-SWNT back contacts (see Supporting Information). J/V curves for s-SWNT/CdTe/CdS/FTO devices where simulated as the Fermi energy of the s-SWNTs was varied from the middle of the band gap to near the valence band edge by increasing the doping level. At the highest level of doping (10^{19} cc^{-1}) the back contact barrier was nearly eliminated and the experimental J/V curves were accurately reproduced. However, the sheet resistance of the prepared films was fairly high (250 Ω/sq), indicating very little doping. Furthermore, experiments designed to investigate the thermal stability of the contact (discussed below) revealed that thoroughly undoped SWNTs also produced good device performance. Thus, it is clear that bulk doping of the SWNT layer is not required to achieve the good performance that is experimentally observed.

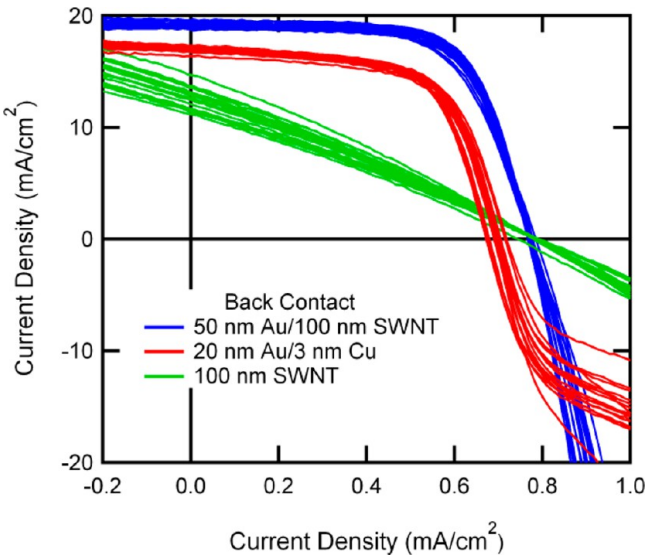

Figure 4. J/V response after heating CdTe devices to 300 °C under Ar flow for 10 min with SWNT (green) and Au/Cu (red) back contacts. The blue curve shows the J/V response for the SWNT-contacted devices after heating and application of 50 nm of Au. Curves for eighteen devices in each category are shown.

The role of SWNT doping and the thermal stability of the copper-free SWNT back contacts were evaluated by comparing the performance of CdTe devices with SWNT and Au/Cu back contacts after heating in flowing Ar at 300 °C for 10 min. J/V curves and key parameters are presented in Figure 4 and Table 1, respectively. The heat treatment causes virtually all dopants to desorb from the SWNT film and increases the sheet resistance of the film to ~600 Ω/□ (see Supporting Information). After the heat treatment, the Au/Cu devices showed a reduced V_{OC} and the rollover behavior that is characteristic of a Schottky barrier at the back contact. The change in the J/V response in comparison to the unheated device (Figure 1) is a classic example of device degradation due to loss of Cu from the back contact interface.[10] In contrast, the SWNT contacted devices exhibit no sign of rollover after the heat treatment. Importantly, the V_{OC} remained high, indicating that the energetics of the band alignment at the SWNT/CdTe back contact are not affected. However, the increased sheet resistance leads to a significantly reduced FF, and the J_{SC} values are substantially lower than for the unheated device (Figure 1) because the effective area over which current is collected by the contacting pin is reduced. The excellent J/V response returns once a thin layer of Au is deposited over the SWNT layer. We note that a heat treatment was also performed on devices that had been overcoated with Au (data not shown). In these cases the Au diffused through the SWNT layer to the CdTe to form a back contact that was dominated by the energetics of a direct Au/CdTe contact (Figure 1). Current efforts in our laboratories are focused on developing metal overlayers with better thermal stability, and reducing the sheet resistance in the neat SWNT films.

In the SCAPS simulations, it was necessary to posit a high doping density for s-SWNTs to reproduce the experimental data. However, the heat treatment studies revealed that high homogeneous doping levels are not required to obtain the correct band alignment needed for a high performance back contact. While the band alignment was suitable prior to deposition of the Au layer, as evidenced by a high V_{OC}, the

dx.doi.org/10.1021/nl402659c | Nano Lett. XXXX, XXX, XXX−XXX

possibility of doping being produced in the SWNT film by the Au was also investigated and found not to be significant (see Supporting Information). On the other hand, the SCAPS simulations could not model the data with explicit consideration of only m-SWNTs under any circumstances. Here, only the work function of the modeled material could be adjusted and no values within reason could be found that reproduced the experimental J/V curves. This result is consistent with expectations that m-SWNTs would behave much like graphite in this context, and produce a rectifying contact if the CdTe were not doped with, for example, Hg or Cu.

A more accurate representation of the physics and chemistry at the interface must deal with local charge distributions, charge transfer interactions, and interface dipoles. Tung has applied the electrochemical potential equalization method developed for molecular species to solid state interfaces and found that surface dipoles associated with bond polarization provide a coherent explanation of both Fermi level pinning and the Schottky barrier height dependence on interface structure.[51] Using similar concepts, first principles density functional calculations showed that the electronic states of s-SWNTs in contact with InAs surfaces could be shifted by more than 0.5 eV in either the positive or negative direction due to interface dipoles.[49] Later, these calculations were confirmed experimentally.[52] Interface dipoles have been evoked more recently by others in describing the behavior of SWNT films on SiO_2 surfaces[53] and in the production of low work function electrodes for organic electronics.[54] In the case of SWNTs on InAs, the direction of the shift of the SWNT band structure depends on whether the InAs surface is reconstructed with In-vacancy or As-vacancy terminations. In effect, the surface dipole produces doping of the SWNT by virtue of dipole-induced charge transfer interactions. The magnitude of the shift of the electronic states expected for s-SWNTs in contact with CdTe surfaces should be comparable to the InAs case due to a similar difference in the Pauling electronegativity for the atomic species in the two materials. Thus, rather than the homogeneous doping that was implemented in the SCAPS modeling, the doping can be done locally at the contacting points by the surface itself. Experimental effort to detect this doping in our samples with Raman and optical absorption spectroscopies have been unsuccessful so far, presumably due to the large volume of SWNTs in the 100 nm thick film that are left unaffected by the surface. However, STM investigations of single SWNTs on InAs surfaces has indeed confirmed the phenomenon.[52]

Interactions between InAs surfaces and the (6,0) m-SWNT were also theoretically investigated.[49] Though the binding mechanism was similar to that determined for (10,0) and (17,0) s-SWNTs, namely a weak chemical bond between the surface cation and the C−C π orbitals of the SWNT, a shift in the electronic band structure was not observed due to strong screening by metallic states that counteracts the dipole effect. These findings validate the intuitive notion that m-SWNTs should behave much like graphite in this context and produce rectifying contacts with CdTe.

Though the calculations were for specific nanotube/semiconductor interfaces that allow the application of periodic boundary conditions, the principles can be generalized to polycrystalline surfaces that present many different types of crystallite facets and surface terminations (see Figure 3). The number of SWNT ends accessible at the film's surface will likely produce many types of contacts, some of which will be of low barrier and therefore dominate the transport. Presently, although more detailed understanding of our experimental findings is required, we tentatively ascribe low barrier behavior to junctions formed by s-SWNT at certain CdTe crystallite facets, while high barrier behavior may be expected for s-SWNTs contacting other crystallite facets where the dipole induced shift in electronic states is of insufficient magnitude or in the wrong direction. Within this "selective contact" model, m-SWNTs are expected to produce relatively high barrier junctions at all interfaces, and not participate significantly in carrier transport.

A direct conclusion of our model is that certain SWNTs are in better electronic equilibrium with the CdTe surface than are others, and that electronic equilibrium between SWNTs in the film is poor. Put differently, the SWNT film does not have one common Fermi energy. The fact that the device contact remains good even after thorough dopant desorption, makes it clear that tube−tube contact and transport is not important to establish low barrier contact. This would not be the case if charge transport across the back of the device needed to occur across multiple tube−tube interfaces, that is, if T were $\gg L$. If the film did have one common Fermi energy, and it had been shifted low enough to provide good overlap with the deep CdTe valence band, then doping would be easily observed for the s-SWNTs in the film via Raman or UV−vis spectroscopies. However, as mentioned previously, this is not the case.

While SWNTs have been of significant interest for PV applications for some time, most effort has been focused on using SWNTs as contacts in organic[55−57] and silicon[53,58,59] devices, or as a replacement for the transparent conducting layers.[56,60] Barnes et al.[61] used the transparency of the SWNT film to form a back contact to a semitransparent CdTe device, but only after a Cu_2Te interfacial layer has been purposefully introduced. For completeness, we note that CdTe and CdS have also been grown directly on patterned, vertically aligned multiwall nanotube forests without the use of copper and photoactive devices were produced.[62] However, this device generated an open circuit voltage of only 7 mV at very high light intensities (see Supporting Information).

This work represents the first example of using SWNTs to make a direct, low barrier electrical contact to a polycrystalline semiconductor thin film without purposeful surface modification. Our analysis suggests that s-SWNTs make direct, barrierless contacts to the individual grains in the polycrystalline CdTe absorber layer and efficiently collect photogenerated charge, while m-SWNTs form rectifying contacts. SWNT films have parallel pathways for conduction through each type of tube in these thin films, so the performance of the s-SWNTs dominates. The SWNT layer is thermally stable and easily applied with a spray process, and the Cu-free SWNT-contacted device shows no signs of degradation during accelerated life testing.

■ ASSOCIATED CONTENT

Ⓢ Supporting Information

Details of optical and low-temperature measurements, calculations of the number of SWNTs that span from the top to the bottom surfaces of the SWNT film, SCAPS modeling, discussion of SWNT doping, and comments on ref 62. This material is available free of charge via the Internet at http://pubs.acs.org.

dx.doi.org/10.1021/nl402659c | Nano Lett. XXXX, XXX, XXX−XXX

AUTHOR INFORMATION

Corresponding Author

*E-mail: Michael.Heben@UToledo.edu.

Notes

The authors declare no competing financial interest.

ACKNOWLEDGMENTS

The authors are grateful for TCO-coated glass samples from Dr. David Strickler, NSG Group (Pilkington North America). This work was supported by the Department of Energy under Award Number DE-SC0006349 and by faculty start-up funds from the University of Toledo.

REFERENCES

(1) http://www.firstsolar.com/.
(2) EPIA global market outlook; http://www.epia.org/home/.
(3) http://www.nrel.gov/ncpv/images/efficiency_chart.jpg (accessed July 10, 2013).
(4) http://www.pv-tech.org/news/nrel_verifies_first_solars_16.1_total_area_module_efficiency_record_leap.
(5) http://files.shareholder.com/downloads/FSLR/1944432606x0x660987/eaff5877-88cd-4a83-9f72-b8b2983cb97f/Q113_Earnings_Call_Presentation_FINAL.pdf.
(6) Fritsche, J.; Kraft, D.; Thissen, A.; Mayer, T.; Klein, A.; Jaegermann, W. *Thin Solid Films* **2002**, *403*, 252−257.
(7) Dobson, K. D.; Visoly-Fisher, I.; Hodes, G.; Cahen, D. *Sol. Energy Mater. Sol. Cells* **2000**, *62* (3), 295−325.
(8) Janik, E.; Triboulet, R. *J. Phys. D: Appl. Phys.* **1983**, *16* (12), 2333−2340.
(9) Yun, J. H.; Kim, K. H.; Lee, D. Y.; Ahn, B. T. *Sol. Energy Mater. Sol. Cells* **2003**, *75* (1−2), 203−210.
(10) Corwine, C. R.; Pudov, A. O.; Gloeckler, M.; Demtsu, S. H.; Sites, J. R. *Sol. Energy Mater. Sol. Cells* **2004**, *82* (4), 481−489.
(11) Demtsu, S. H.; Albin, D. S.; Sites, J. R.; Metzger, W. K.; Duda, A. *Thin Solid Films* **2008**, *516* (8), 2251−2254.
(12) Berniard, T. J.; Albin, D. S.; To, B.; Pankow, J. W.; Young, M.; Asher, S. E. *J. Vac. Sci. Technol., B* **2004**, *22* (5), 2423−2428.
(13) Strevel, N.; Trippel, L.; Gloeckler, M. *Photovoltaics Int.* **2012**, *17* (3), 1−3.
(14) Branker, K.; Pathak, M. J. M.; Pearce, J. M. *Renewable Sustainable Energy Rev.* **2011**, *15* (9), 4470−4482.
(15) NOTE: A single levelized cost of electricity calculation requires a particular value of the discount rate to be assumed to determine the net present value of all terms. This number is not well-known especially when long time periods are considered. A comparison between LCOE's of only slightly different technologies is straightforward. In our case, we simply considered the yearly energy production for a 14% efficient module operating in Toledo, OH and compared the LCOE with and without observed efficiency degradations.
(16) Romeo, N.; Bosio, A.; Tedeschi, R.; Romeo, A.; Canevari, V. *Sol. Energy Mater. Sol. Cells* **1999**, *58* (2), 209−218.
(17) Batzner, D. L.; Romeo, A.; Terheggen, M.; Dobeli, M.; Zogg, H.; Tiwari, A. N. *Thin Solid Films* **2004**, *451*, 536−543.
(18) Compaan, A. D.; Gupta, A.; Lee, S. Y.; Wang, S. L.; Drayton, J. *Sol. Energy* **2004**, *77* (6), 815−822.
(19) Spath, B.; Fritsche, J.; Sauberlich, F.; Klein, A.; Jaegermann, W. *Thin Solid Films* **2005**, *480*, 204−207.
(20) Lin, H.; Xia, W.; Wu, H. N.; Tang, C. W. *Appl. Phys. Lett.* **2010**, *97* (12), 123504.
(21) Lin, H.; Irfan, A.; Xia, W.; Wu, H. N.; Gao, Y. L.; Tang, C. W. *Sol. Energy Mater. Sol. Cells* **2012**, *99*, 349−355.
(22) Khrypunov, G.; Romeo, A.; Kurdesau, F.; Batzner, D. L.; Zogg, H.; Tiwari, A. N. *Sol. Energy Mater. Sol. Cells* **2006**, *90* (6), 664−677.
(23) Abken, A. E. *Sol. Energy Mater. Sol. Cells* **2002**, *73* (4), 391−409.
(24) Gupta, A.; Compaan, A. D. *Appl. Phys. Lett.* **2004**, *85* (4), 684−686.
(25) Plotnikov, V.; Liu, X.; Paudel, N.; Kwon, D.; Wieland, K. A.; Compaan, A. D. *Thin Solid Films* **2011**, *519* (21), 7134−7137.
(26) Unpublished Results.
(27) Dillon, A. C.; Parilla, P. A.; Alleman, J. L.; Perkins, J. D.; Heben, M. J. *Chem. Phys. Lett.* **2000**, *316* (1−2), 13−18.
(28) Nishide, D.; Miyata, Y.; Yanagi, K.; Tanaka, T.; Kataura, H. *Jpn. J. Appl. Phys.* **2009**, *48* (1), 015004.
(29) Wu, Z. C.; Chen, Z. H.; Du, X.; Logan, J. M.; Sippel, J.; Nikolou, M.; Kamaras, K.; Reynolds, J. R.; Tanner, D. B.; Hebard, A. F.; Rinzler, A. G. *Science* **2004**, *305* (5688), 1273−1276.
(30) Tenent, R. C.; Barnes, T. M.; Bergeson, J. D.; Ferguson, A. J.; To, B.; Gedvilas, L. M.; Heben, M. J.; Blackburn, J. L. *Adv. Mater.* **2009**, *21* (31), 3210−3216.
(31) Niemegeers, A.; Burgelman, M. *J. Appl. Phys.* **1997**, *81* (6), 2881−2886.
(32) Gessert, T. A.; Mason, A. R.; Sheldon, P.; Swartzlander, A. B.; Niles, D.; Coutts, T. J. *J. Vac. Sci. Technol., A* **1996**, *14* (3), 806−812.
(33) Faykosh, G. Personal Communication.
(34) Bätzner, D. L.; Romeo, A.; Zogg, H.; Tiwari, A. N. *'CdTe/CdS solar cells performance under low irradiance', Proceedings of the 17th European Photovoltaic Solar Energy Conference and Exhibition, Munich*, McNelis, B.; Palz, W.; Ossenbrink, H. A.; Helm, P., Eds.; WIP-Renewable Energies, 2001, 1180−1183.
(35) Rau, U. *Appl. Phys. Lett.* **1999**, *74* (1), 111−113.
(36) Zhang, Y.; Franklin, N. W.; Chen, R. J.; Dai, H. J. *Chem. Phys. Lett.* **2000**, *331* (1), 35−41.
(37) Albin, D.; Levi, D.; Asher, S.; Balcioglu, A.; Dhere, R.; Hiltner, J. IEEE, Precontact surface chemistry effects on CdS/CdTe solar cell performance and stability. In *Conference Record of the Twenty-Eighth IEEE Photovoltaic Specialists Conference - 2000*; IEEE: New York, 2000; pp 583−586.
(38) Bi, H.; Huang, F. Q.; Liang, J.; Xie, X. M.; Jiang, M. H. *Adv. Mater.* **2011**, *23* (28), 3202−3206.
(39) Lin, T. Q.; Huang, F. Q.; Liang, J.; Wang, Y. X. *Energy Environ. Sci.* **2011**, *4* (3), 862−865.
(40) Liang, J.; Bi, H.; Wan, D. Y.; Huang, F. Q. *Adv. Funct. Mater.* **2012**, *22* (6), 1267−1271.
(41) Zhu, H. W.; Wei, J. Q.; Wang, K. L.; Wu, D. H. *Sol. Energy Mater. Sol. Cells* **2009**, *93* (9), 1461−1470.
(42) McDonald, T. J.; Svedruzic, D.; Kim, Y. H.; Blackburn, J. L.; Zhang, S. B.; King, P. W.; Heben, M. J. *Nano Lett.* **2007**, *7* (11), 3528−3534.
(43) Blackburn, J. L.; Barnes, T. M.; Beard, M. C.; Kim, Y. H.; Tenent, R. C.; McDonald, T. J.; To, B.; Coutts, T. J.; Heben, M. J. *ACS Nano* **2008**, *2* (6), 1266−1274.
(44) Saito, R.; Fujita, M.; Dresselhaus, G.; Dresselhaus, M. S. *Appl. Phys. Lett.* **1992**, *60* (18), 2204−2206.
(45) Dan, B.; Ma, A. W. K.; Haroz, E. H.; Kono, J.; Pasquali, M. *Ind. Eng. Chem. Res.* **2012**, *51* (30), 10232−10237.
(46) Barnes, T. M.; Blackburn, J. L.; van de Lagemaat, J.; Coutts, T. J.; Heben, M. J. *ACS Nano* **2008**, *2* (9), 1968−1976.
(47) Kim, S.; Yim, J.; Wang, X.; Bradley, D. D. C.; Lee, S.; Demello, J. C. *Adv. Funct. Mater.* **2010**, *20* (14), 2310−2316.
(48) Burgelman, M.; Nollet, P.; Degrave, S. *Thin Solid Films* **2000**, *361*, 527−532.
(49) Kim, Y. H.; Heben, M. J.; Zhang, S. B. *Phys. Rev. Lett.* **2004**, *92* (17), 176102.
(50) Hennrich, F.; Wellmann, R.; Malik, S.; Lebedkin, S.; Kappes, M. M. *Phys. Chem. Chem. Phys.* **2003**, *5* (1), 178−183.
(51) Tung, R. T. *Phys. Rev. B* **2001**, *64* (20), 205310.
(52) Ruppalt, L. B.; Albrecht, P. M.; Lyding, J. W. *J. Phys. IV* **2006**, *132*, 31−34.
(53) Wadhwa, P.; Liu, B.; McCarthy, M. A.; Wu, Z. C.; Rinzler, A. G. *Nano Lett.* **2010**, *10* (12), 5001−5005.
(54) Zhou, Y.; Fuentes-Hernandez, C.; Shim, J.; Meyer, J.; Giordano, A. J.; Li, H.; Winget, P.; Papadopoulos, T.; Cheun, H.; Kim, J.; Fenoll, M.; Dindar, A.; Haske, W.; Najafabadi, E.; Khan, T. M.; Sojoudi, H.; Barlow, S.; Graham, S.; Bredas, J.-L.; Marder, S. R.; Kahn, A.; Kippelen, B. *Science* **2012**, *336* (6079), 327−332.

(55) Barnes, T. M.; Bergeson, J. D.; Tenent, R. C.; Larsen, B. A.; Teeter, G.; Jones, K. M.; Blackburn, J. L.; van de Lagemaat, J. *Appl. Phys. Lett.* **2010**, *96* (24), 243309.
(56) van de Lagemaat, J.; Barnes, T. M.; Rumbles, G.; Shaheen, S. E.; Coutts, T. J.; Weeks, C.; Levitsky, I.; Peltola, J.; Glatkowski, P. *Appl. Phys. Lett.* **2006**, *88* (23), 233503.
(57) Cataldo, S.; Salice, P.; Menna, E.; Pignataro, B. *Energy Environ. Sci* **2012**, *5* (3), 5919−5940.
(58) Jia, Y.; Li, P. X.; Wei, J. Q.; Cao, A. Y.; Wang, K. L.; Li, C. L.; Zhuang, D. M.; Zhu, H. W.; Wu, D. H. *Mater. Res. Bull.* **2010**, *45* (10), 1401−1405.
(59) Ong, P.-L.; Euler, W. B.; Levitsky, I. A. *Nanotechnology* **2010**, *21* (10), 105203.
(60) Contreras, M. A.; Barnes, T.; van de Lagemaat, J.; Rumbles, G.; Coutts, T. J.; Weeks, C.; Glatkowski, P.; Levitsky, I.; Peltola, J.; Britz, D. A. *J. Phys. Chem. C* **2007**, *111* (38), 14045−14048.
(61) Barnes, T. M.; Wu, X.; Zhou, J.; Duda, A.; van de Lagemaat, J.; Coutts, T. J.; Weeks, C. L.; Britz, D. A.; Glatkowski, P. *Appl. Phys. Lett.* **2007**, *90* (24), 243503.
(62) Camacho, R. E.; Morgan, A. R.; Flores, M. C.; McLeod, T. A.; Kumsomboone, V. S.; Mordecai, B. J.; Bhattacharjea, R.; Tong, W.; Wagner, B. K.; Flicker, J. D.; Turano, S. P.; Ready, W. J. *J. Mater.* **2007**, *59* (3), 39−42.